Supplementary Information

Degradation of ancient Maya carved tuff stone at Copan and its bacterial bioconservation

Kerstin Elert, Encarnación Ruiz-Agudo, Fadwa Jroundi, Maria Teresa Gonzalez-Muñoz, Barbara W. Fash, William L. Fash, Nieves Valentin, Alberto de Tagle and Carlos Rodriguez-Navarro*

*Corresponding author. Email: carlosrn@ugr.es

This file includes:

Supplementary Note 1

Calculation of critical flaw length

According to Wangler *et al.*[1], buckling results from the suppression of the free swelling strain ε of a thin layer of stone over a flaw located at a depth t below the exposed surface, with width L. Buckling thus occurs when the compressive stress σ in the plane of the wet layer,

$$\sigma = \frac{E\varepsilon}{1-\upsilon^2} \qquad (1)$$

is equal to the critical buckling stress, σ_c,

$$\sigma_c = \frac{E}{1-\upsilon^2}\frac{\pi^2}{3A_c^2} \qquad (2)$$

where E is the elastic modulus, υ is the Poisson´s ratio, and A_c is the critical aspect ratio L/t where buckling occurs. Combining eqs. (1) and (2), the critical aspect ratio is defined in terms of the free swelling strain:

$$A_c = \frac{\pi}{\sqrt{3\varepsilon}} \qquad (3)$$

It is thus possible to determine A_c knowing the free swelling strain, ε, and, knowing the depth of the flaw, t, it is also possible to determine the critical flaw length L. In our case, the thickness of tuff stone scales (determined in thin sections cut normal to the stone, as well as measuring scales that fell off the stone surfaces at Copan) was ~0.5-3 mm. Using eq. (3), critical flaw lengths L of 14.5 mm up to 87.1 mm are calculated for the smallest and largest scale thickness, considering the average ε value of 0.0039 determined here.

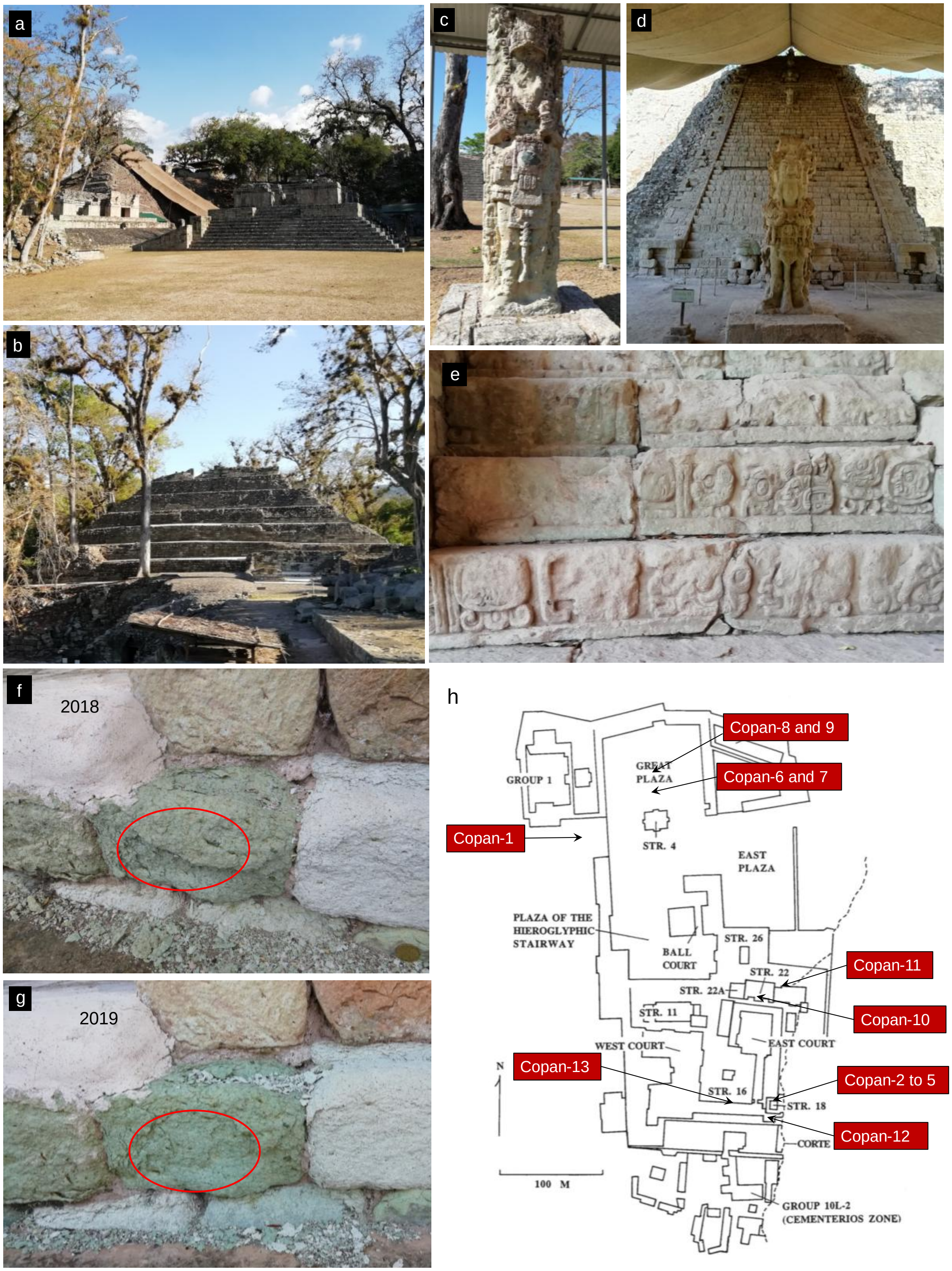

Supplementary Figure 1. Different views of the Maya site of Copan and samples' location: (a) and (b) Principal Group, Ballcourt Structures 10L-9 and 10, and Structure 10L-26; Structure

10L-16. (c) Stela 3. (d) The Hieroglyphic Stairway and Stela M (with the canvas shelter). (e) Detail of differential weathering of the step risers at the Hieroglyphic Stairway. Note that the carved relief is perfectly legible in some sections of the step risers, while it is completely lost in other sections, such as the upper riser, and the left part of the middle riser; (f) and (g) Images of tuff stone blocks at Structure 10L-18 taken in 2018 and 2019. Note the loss of a large scale after 1 y elapsed time (area marked by the red ellipse). (h) general plan of the Copan site Principal Group, 10L-1 (after Webster[2]), showing the location of the collected tuff stone samples: Copan 1 is a decontextualized tuff stone block; Samples Copan 2 and 4 correspond to scales collected from two stone blocks at Structure 10L-18 selected for *in situ* treatment trials, whereas Copan 3 and 5 correspond samples collected from two adjacent stone blocks at Structure 10L-18 left untreated; Copan 6 and 7 and Copan 8 and 9 correspond to scales from Stela 4 and Stela C (CE 711), respectively, both located in the Great Plaza; Sample 10 is a highly degraded stone from Structure 10L-22; Sample 11 is a highly degraded decontextualized stone block close to Structure 10L-22; Sample 12 is a partially degraded decontextualized stone block close to the access to Structure 10L-16; Sample 13 corresponds to a decontextualized tuff block collected close to the entrance of the tunnel in Structure 10L-16, with negligible deterioration.

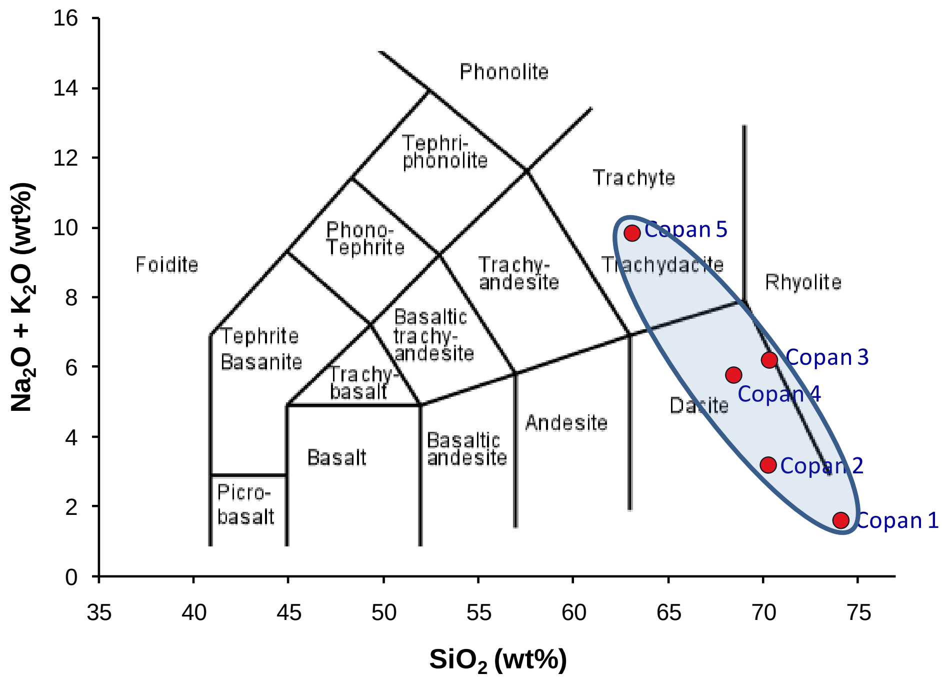

Supplementary Figure 2. Composition of Copan tuff stone. Composition plotted on a Le Bas *et al*.[3] diagram for volcanic rocks. The blue colored area marks the compositional variation of the tuff stone, indicating its trachydacitic-rhyodacitic volcaniclastic nature.

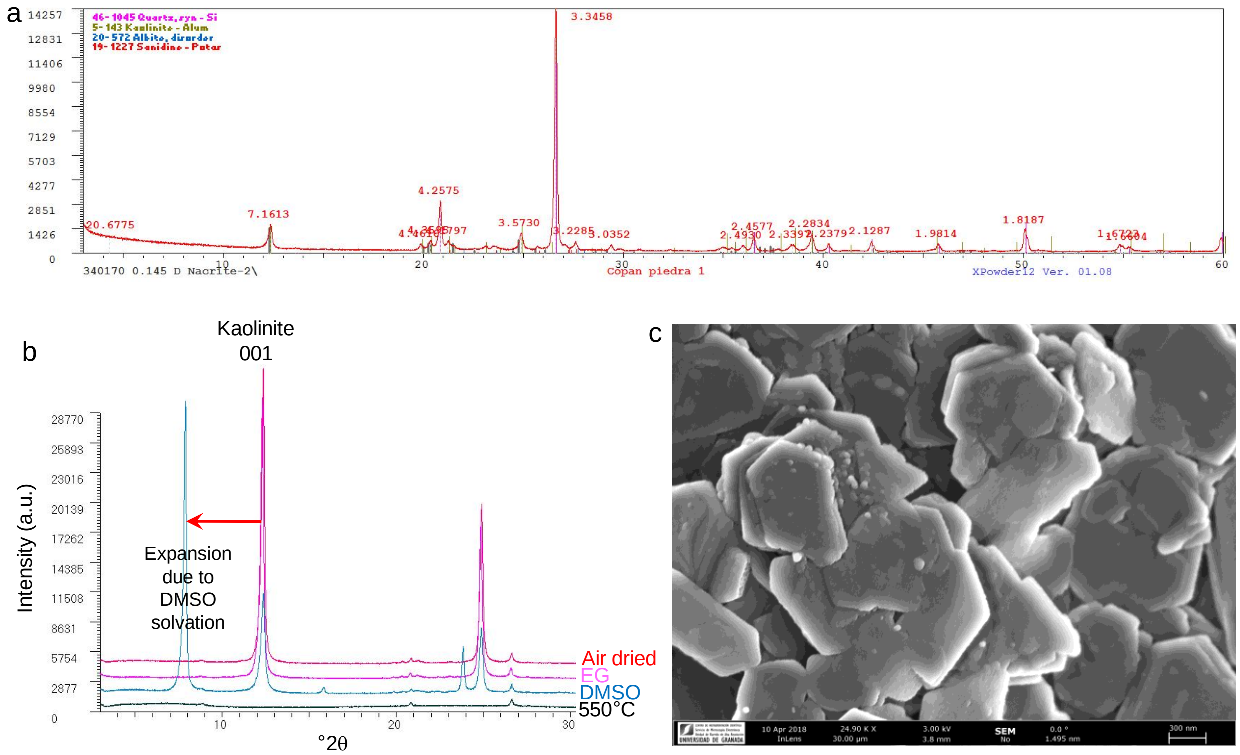

Supplementary Figure 3. Mineralogy of the bulk and clay fraction of Copan 1 (tuff stone Type 1): a) XRD pattern of the bulk tuff stone, showing abundant kaolinite and quartz along with minor proportions of sanidine and albite; b) XRD patterns of the clay fraction air dried, EG and DMSO solvated, and heat treated to 550°C. Note the shift of the 001 Bragg peak of kaolinite to a lower 2θ angle upon DMSO solvation, and the disappearance of kaolinite Bragg peaks after heat treatment; c) FESEM image of kaolinite crystals with the common hexagonal plate-like morphology.

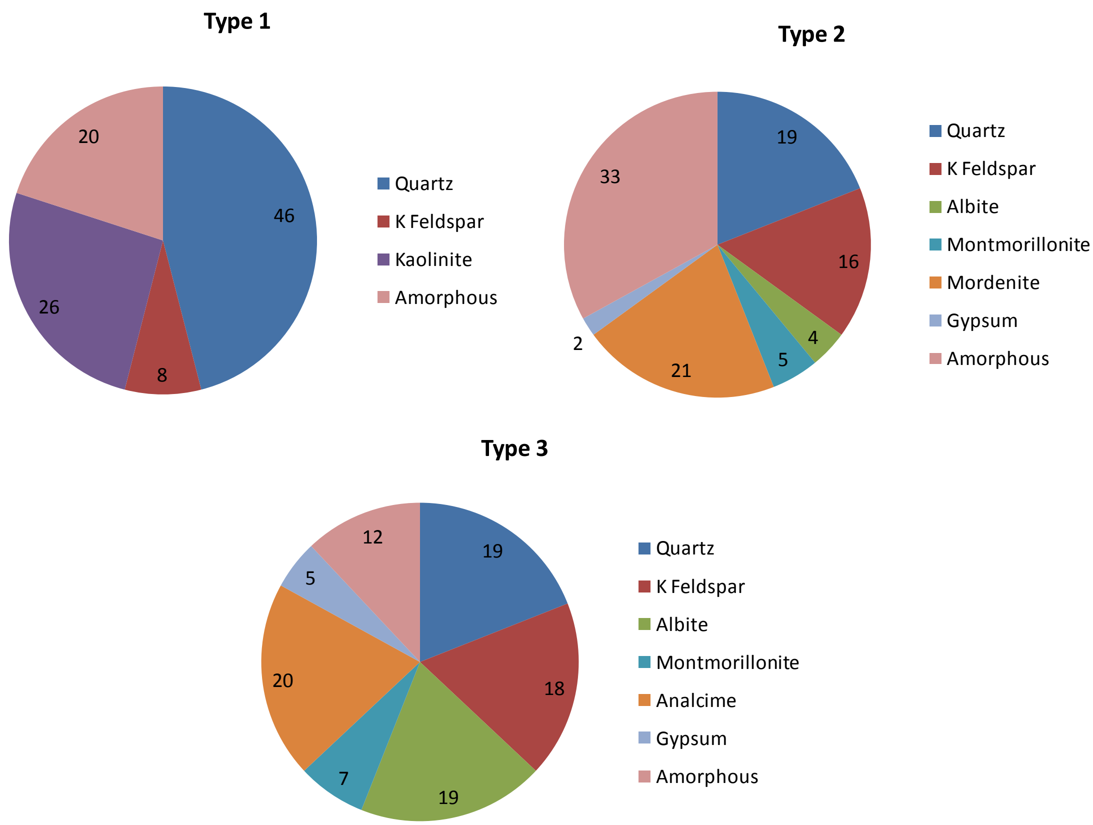

Supplementary Figure 4. Representative results of the quantitative XRD analysis using the Rietveld method (with metallic Si internal standard) of the different types of Copan stones.

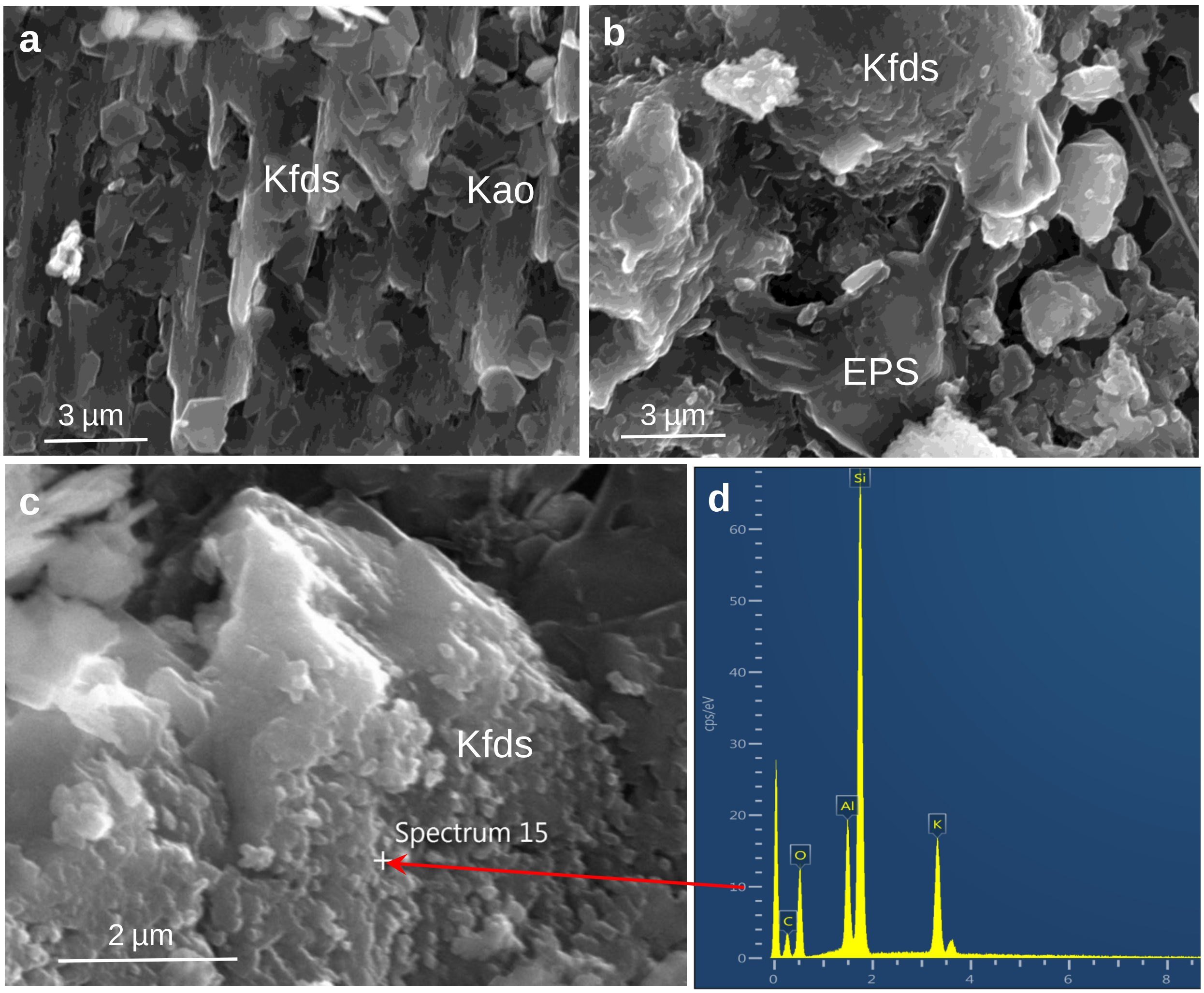

Supplementary Figure 5. FESEM-EDS analysis of weathered Copan stone. . a) Corroded K feldspar (Kfds) phenocrystals, along kaolinite plates (Kao) in Type 1 tuff stone; b) Corroded sanidine surrounded by bacterial EPS in Type 2 stone; c) Heavily corroded K-feldspar (Kfds) surrounded by bacterial EPS in Type 2 stone; d) EDS spectrum of the K-feldspar in (c). The red arrow shows the analyzed spot.

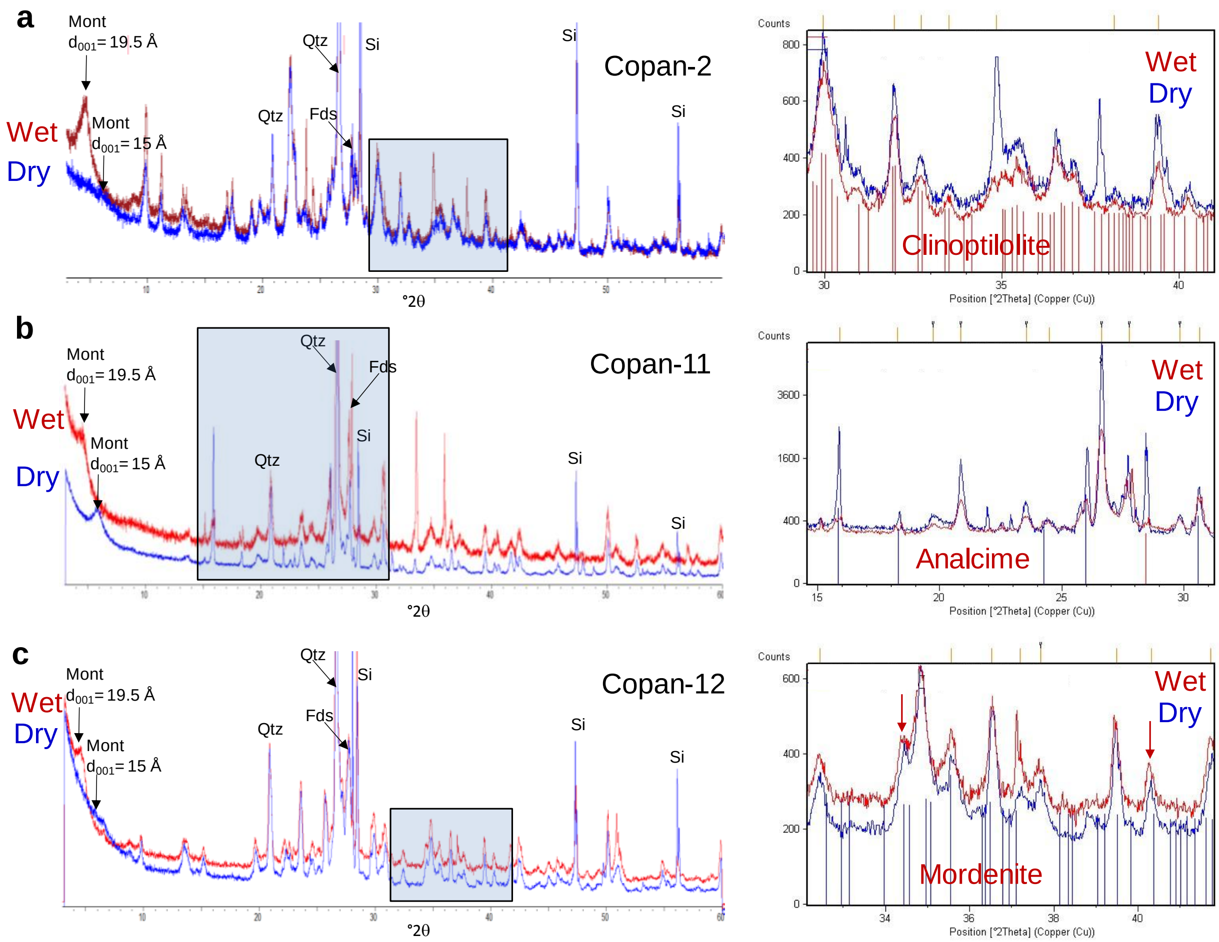

Supplementary Figure 6. XRD analysis of dry and wet Copan stone samples with different zeolites. a) Copan-2 including clinoptilolite (Type 2); b) Copan-11 including analcime (Type 3); and c) Copan-12 including mordenite (Type 2). The XRD patterns on the left show the full 2θ explored range for the dry and wet samples, whereas the patterns on the right show the selected area indicated by the shaded region on the left. The vertical bars in the patterns on the right show the position of the Bragg peaks of the corresponding zeolite. The red arrows in the selected area in (c) point to right-shifted Bragg peaks of wet mordenite (as compared with those of dry mordenite). Legend: Mont, montmorillonite; Qtz, quartz; Fds, feldspars; Si, silicon (internal standard). The peaks not labeled correspond to zeolite phases. Note the systematic large shift to lower 2θ values (i.e., higher d_{001}-spacing) of montmorillonite 001 Bragg peak after wetting.

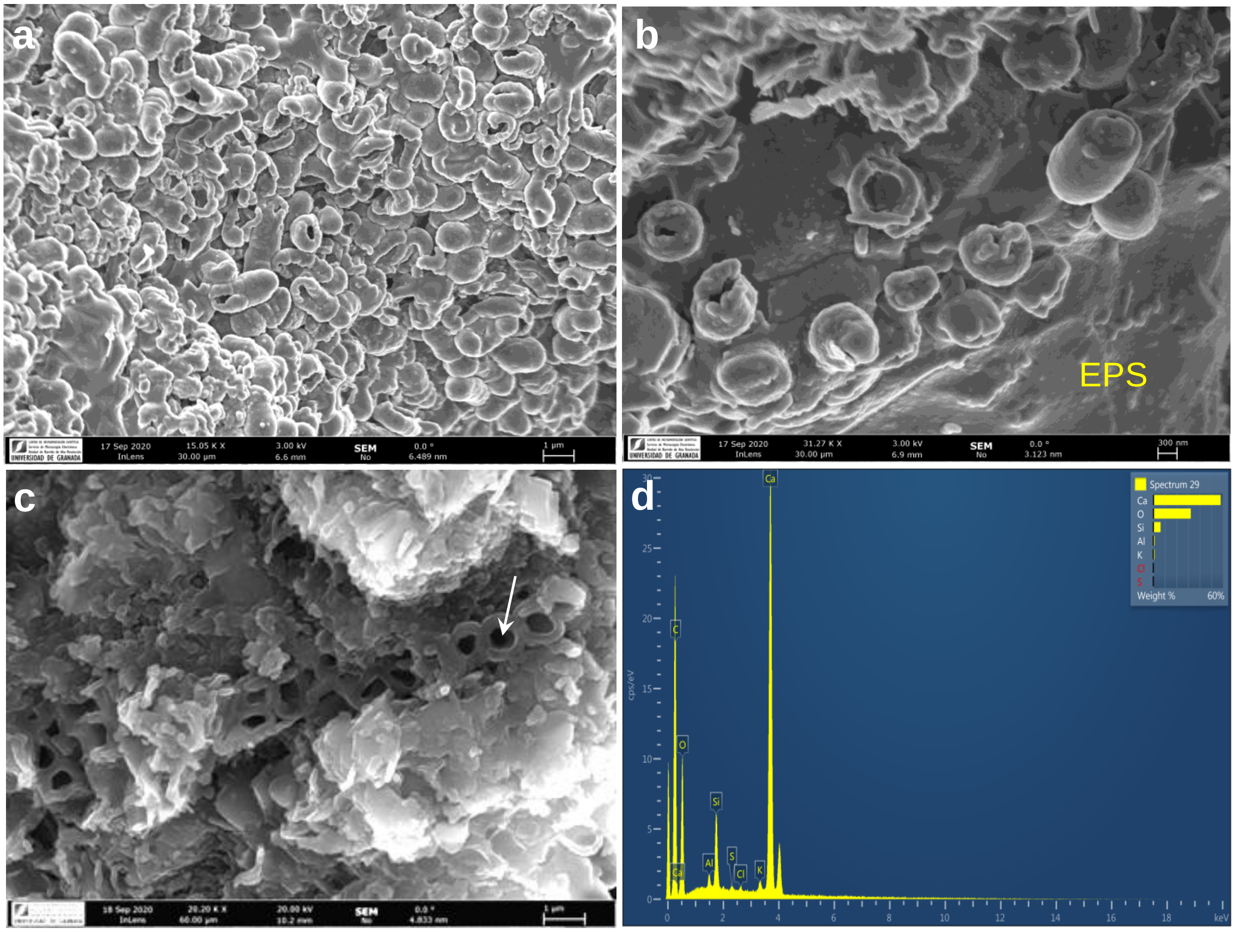

Supplementary Figure 7. FESEM images of bacterially treated Copan stone. a) Aspect of the surface of a buff-greenish Copan stone block treated in the laboratory showing massive calcification of bacterial cell. In this case, a color change ΔE ~8 was observed. Note that such a massive proliferation of carbonatogenic bacteria and the resultant calcification was only observed in this particular treated sample (Copan 13); b) Calcified bacterial cells embedded in EPS in Copan stone treated *in situ*; c) Aspect of the fracture surface of Copan stone treated in the laboratory showing calcified bacterial cells (with a hollow core; see arrow) welded among them and with the silicate matrix; d) EDS spectrum of calcified bacterial cells in (c), showing that C and Ca are the main elements in these structures, consistent with the formation of $CaCO_3$.

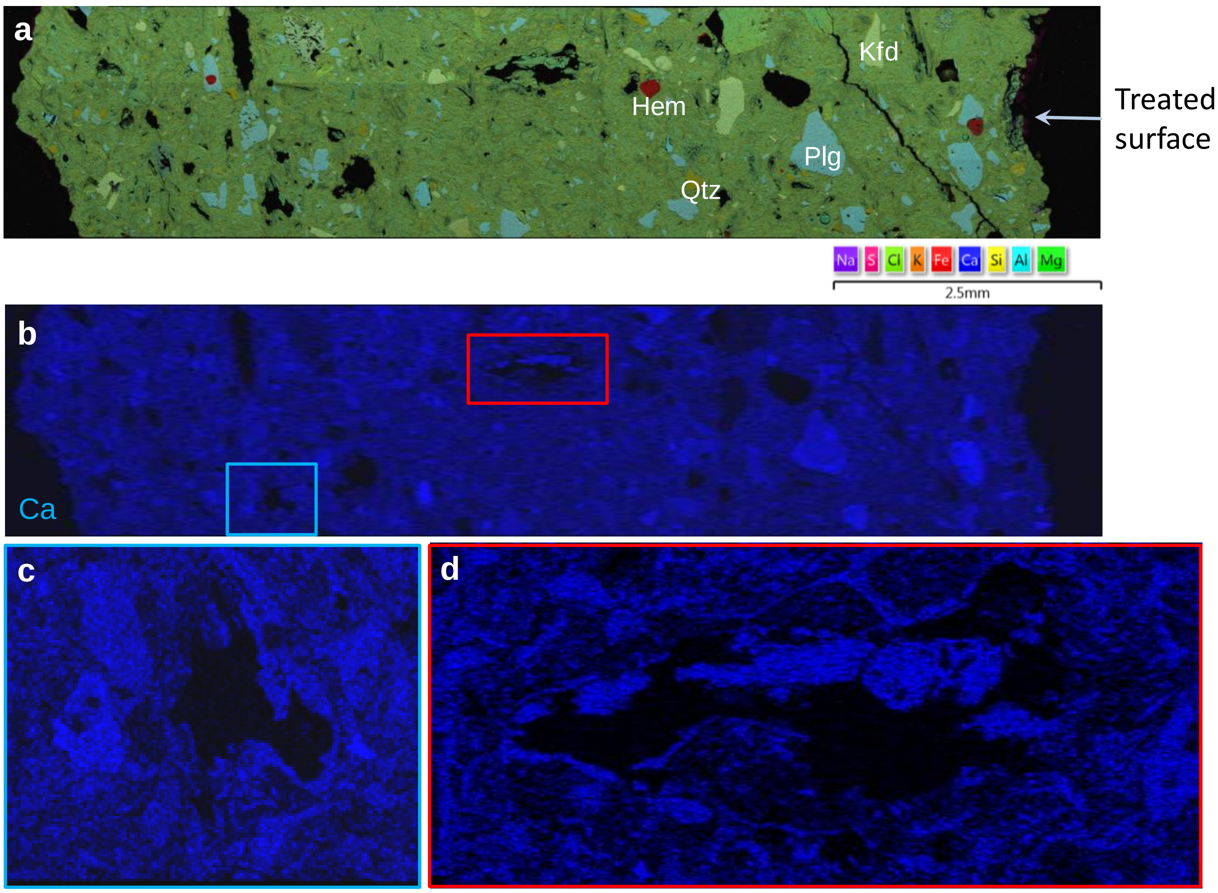

Supplementary Figure 8. EDS elemental mapping of a thin section cut normal to the treated surface of Copan stone. a) Overall elemental map. Phenocrystals of quartz (Qtz), K-feldspar (Kfd), plagioclase (Plg) and hematite (Hem) are indicated; b) Map of Ca distribution; c) and d) enlarged blue and red squared area in (b). The brighter blue areas lining the pores (black areas) correspond to bacterial calcium carbonate.

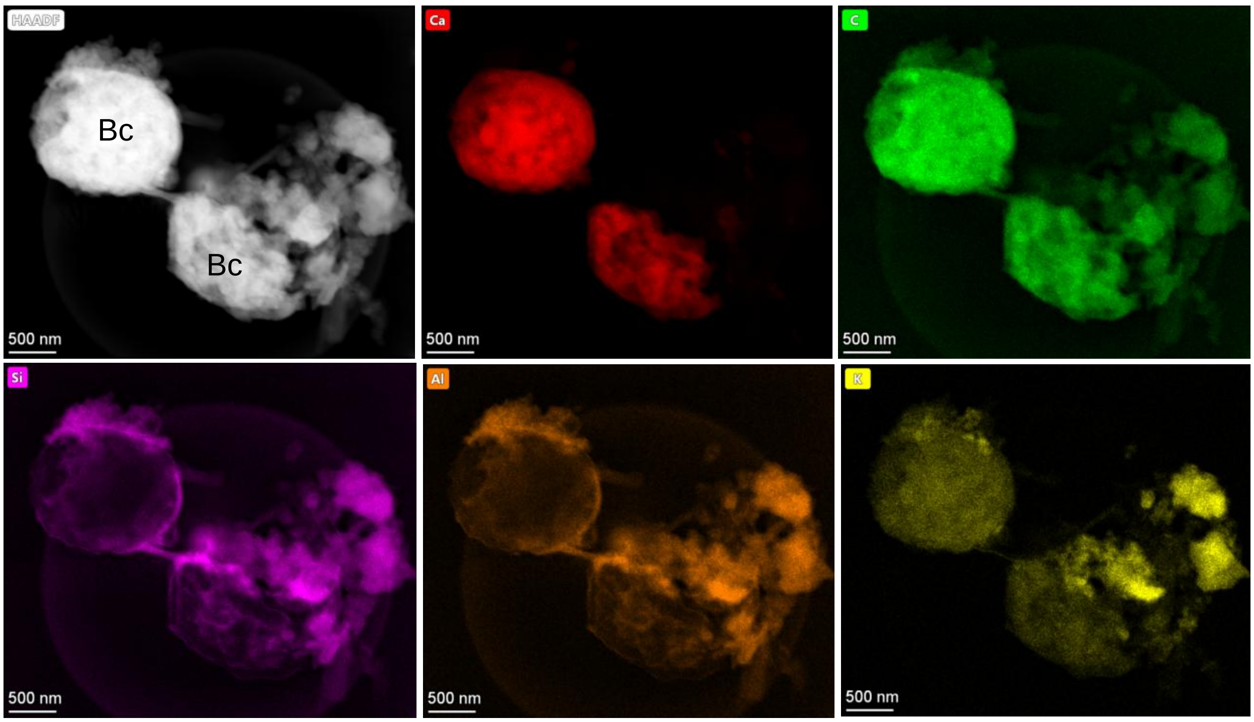

Supplementary Figure 9. TEM-AEM analysis of treated Copan stone. HAADF images and corresponding elemental maps of calcified bacterial cells (Bc), along with aluminosilicate mineral particles in laboratory treated Copan stone (Copan 12).

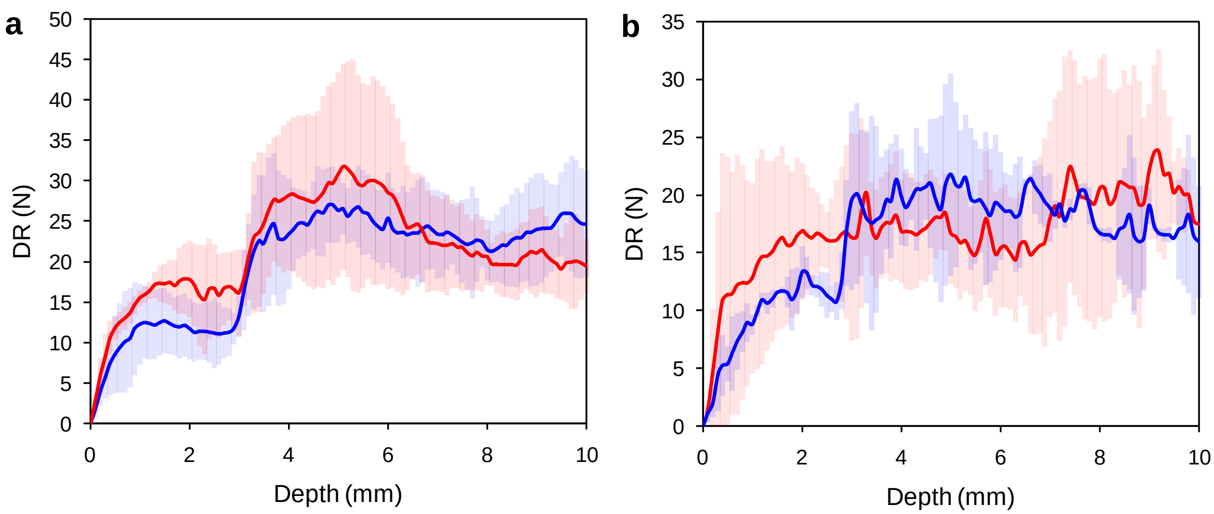

Supplementary Figure 10. Drilling resistance (DR) of Copan stone before and after bacterial treatment in the laboratory: s) Copan stone Type 2 (Copan 13; block with minimal decay); b) Copan stone Type 3 (Copan 11; highly decayed stone block). Blue line: average values (*N*=5) before treatment; Red line: average values (*N*=6) after treatment. Shaded areas show standard deviation.

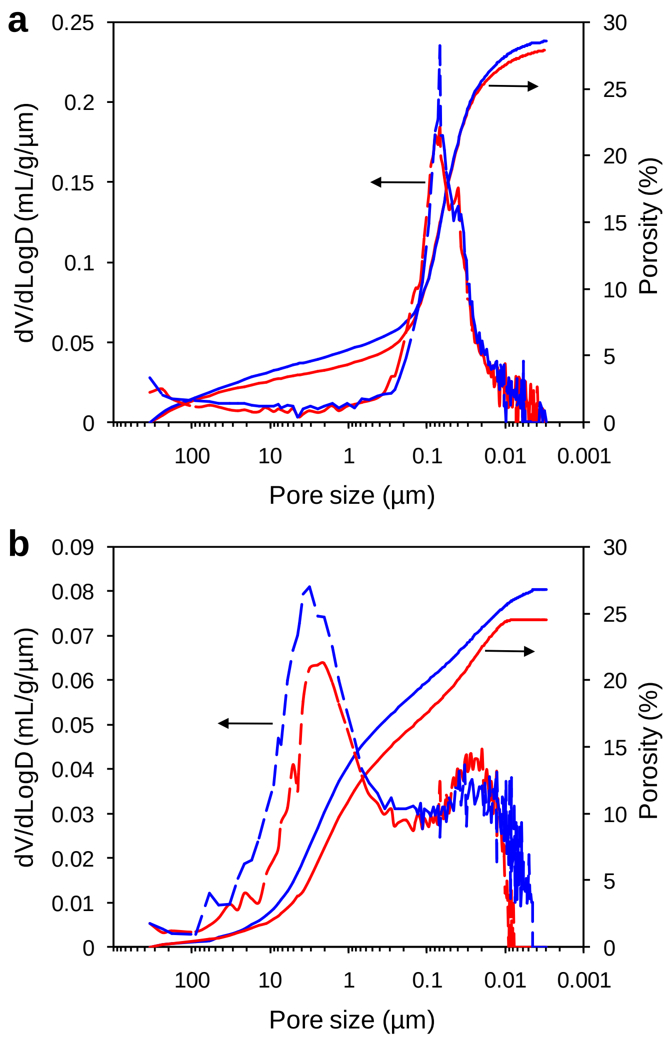

Supplementary Figure 11. Porosity and pore size distribution of Copan stone. Representative MIP plots showing both the cumulative intrusion curves (i.e., porosity) and pore size distribution curves (i.e., log of differential intrusion, or d*V*/dLog*D*, vs. pore size, where *V* is the intruded volume and *D* is the pore diameter) for untreated (blue lines) and treated (red lines) stone blocks from Structure 10L-18 (a) and sample Copan-11, before and after treatment in the laboratory (b).

Supplementary Table 1. Chemical composition of Copan tuff stones (wt% oxides) based on XRF analysis

	Copan 1	Copan 2	Copan 3	Copan 4	Copan 5
SiO_2	74.08	70.25	70.35	68.43	63.13
Al_2O_3	14.58	13.47	12.56	11.93	16
Fe_2O_3	1.58	1.49	2.14	1.86	4
MnO	0.02	0.02	0.01	0.02	0.01
MgO	0.17	0.92	0.44	0.37	0.97
CaO	1.26	3.3	2.75	4.4	1.57
Na_2O	0.2	1.23	1.76	1.85	1.2
K_2O	1.39	1.96	4.44	3.91	8.63
TiO_2	0.28	0.19	0.16	0.17	0.33
P_2O_5	0.11	0.03	0.03	0.03	0.03
LOI	5.97	6.73	4.87	6.59	3.66
Total	99.64	99.59	99.51	99.56	99.53

Supplementary Table 2. Color changes of Copan stone after bacterial treatment in the laboratory

		Before treatment			After treatment			
Stone variety		L*	a*	b*	L*	a*	b*	ΔE
Green	Average (*N*=22)	68.0	-4.3	12.9	67.2	-4.4	15.3	2.6
	Stdev	2.2	1.0	1.4	1.9	1.5	1.8	0.7
Buff-Greenish	Average (*N*=19)	74.1	-3.0	15.8	80.0	-1.9	9.3	8.8
	Stdev	0.8	0.2	1.0	0.9	0.1	0.6	0.4

Supplementary References

1. Wangler, T. P., Stratulat, A., Duffus, P., Prévost, J. H. & Scherer, G. W. Flaw propagation and buckling in clay-bearing sandstones. *Environm. Earth Sci*. **63**, 1565-1572 (2011).
2. Webster, D. The archaeology of Copan, Honduras. *J. Archaeol. Res*. **7**, 1-53 (1999).
3. Le Bas, M., Le Maitre, R., Streckeisen, A. & Zanettin, B. IUGS Subcommission on the Systematics of Igneous Rocks, A chemical classification of volcanic rocks based on the total alkali-silica diagram. *J. Petrology* **27**, 745-750 (1986).